



HAL
open science

Two-scale ion meandering caused by the polarization electric field during asymmetric reconnection

Shan Wang, Li-Jen Chen, Michael Hesse, Naoki Bessho, Daniel J. Gershman, John Dorelli, Barbara Giles, Roy B. Torbert, Craig J. Pollock, Robert Strangeway, et al.

► **To cite this version:**

Shan Wang, Li-Jen Chen, Michael Hesse, Naoki Bessho, Daniel J. Gershman, et al.. Two-scale ion meandering caused by the polarization electric field during asymmetric reconnection. *Geophysical Research Letters*, 2016, 43, pp.7831-7839. 10.1002/2016GL069842 . insu-03669453

HAL Id: insu-03669453

<https://insu.hal.science/insu-03669453>

Submitted on 17 May 2022

HAL is a multi-disciplinary open access archive for the deposit and dissemination of scientific research documents, whether they are published or not. The documents may come from teaching and research institutions in France or abroad, or from public or private research centers.

L'archive ouverte pluridisciplinaire **HAL**, est destinée au dépôt et à la diffusion de documents scientifiques de niveau recherche, publiés ou non, émanant des établissements d'enseignement et de recherche français ou étrangers, des laboratoires publics ou privés.

Copyright



RESEARCH LETTER

10.1002/2016GL069842

Key Points:

- Ions have two scales of meandering motion close to the X line, dominantly trapped by the electric and magnetic force, respectively
- Ion distributions exhibit counter-streaming beams and crescent shapes in inner and outer scales, leading to separate nongyrotropy peaks
- Counter-streaming and crescent ion distributions are observed by MMS in magnetopause reconnection diffusion regions

Supporting Information:

- Supporting Information S1

Correspondence to:

S. Wang,
swang90@umd.edu

Citation:

Wang, S., et al. (2016), Two-scale ion meandering caused by the polarization electric field during asymmetric reconnection, *Geophys. Res. Lett.*, *43*, 7831–7839, doi:10.1002/2016GL069842.

Received 31 MAY 2016

Accepted 19 JUL 2016

Accepted article online 28 JUL 2016

Published online 13 AUG 2016

Two-scale ion meandering caused by the polarization electric field during asymmetric reconnection

Shan Wang^{1,2}, Li-Jen Chen^{1,2}, Michael Hesse², Naoki Bessho^{1,2}, Daniel J. Gershman², John Dorelli², Barbara Giles², Roy B. Torbert³, Craig J. Pollock², Robert Strangeway⁴, Robert E. Ergun⁵, James L. Burch⁶, Levon Avanov², Benoit Lavraud^{7,8}, Thomas E. Moore², and Yoshifumi Saito⁹

¹Astronomy Department, University of Maryland, College Park, Maryland, USA, ²NASA Goddard Space Flight Center, Greenbelt, Maryland, USA, ³Space Science Center, University of New Hampshire, Durham, New Hampshire, USA, ⁴Department of Earth, Planetary, and Space Sciences, University of California, Los Angeles, California, USA, ⁵Laboratory for Atmospheric and Space Physics, University of Colorado Boulder, Boulder, Colorado, USA, ⁶Southwest Research Institute San Antonio, San Antonio, Texas, USA, ⁷Institut de Recherche en Astrophysique et Planétologie, Université de Toulouse, Toulouse, France, ⁸Centre National de la Recherche Scientifique, UMR 5277, Toulouse, France, ⁹Institute for Space and Astronautical Science, Sagami-hara, Japan

Abstract Ion velocity distribution functions (VDFs) from a particle-in-cell simulation of asymmetric reconnection are investigated to reveal a two-scale structure of the ion diffusion region (IDR). Ions bouncing in the inner IDR are trapped mainly by the electric field normal to the current sheet (N direction), while those reaching the outer IDR are turned back mainly by the magnetic force. The resulting inner layer VDFs have counter-streaming populations along N with decreasing counter-streaming speeds away from the midplane while maintaining the out-of-plane speed, and the outer layer VDFs exhibit crescent shapes toward the out-of-plane direction. Observations of the above VDF features and the normal electric fields provide evidence for the two-scale meandering motion.

1. Introduction

During magnetic reconnection, the decoupling of plasmas from the magnetic field occurs in the diffusion region. During the meandering motion around the reversal reconnecting magnetic field (along L) and the cyclotron turning around the reconnected magnetic field (along N), particles get accelerated by the out-of-plane (M) reconnection electric field (L , M , and N form an orthogonal coordinate), convert the bulk energy to the outflow direction, and are thermalized through gyrotropization and pitch angle scattering [e.g., Chen et al., 2011; Bessho et al., 2014; Shuster et al., 2015; Liu et al., 2015; Lavraud et al., 2016].

With electrons getting access closer to the current sheet midplane, a polarization Hall electric field in N pointing toward the midplane is built up due to the charge separation [e.g., Fujimoto, 2006; Chen et al., 2012]. Simulations [Aunai et al., 2011] and observations [Wygant et al., 2005] suggested that the ion motion in the reconnection exhaust is mainly governed by the in-plane electrostatic potential instead of the magnetic force. Ions are trapped near the midplane by E_N and are accelerated by E_L . The work by Wygant et al. [2005] and Aunai et al. [2011] triggered the question whether the trapping by the magnetic force and the acceleration by the reconnection electric field are important for ions.

The E_N structure in symmetric reconnection is modified in asymmetric reconnection. The magnetosheath-pointing E_N can extend to the magnetosheath side of the magnetic field reversal, supported by the electron pressure gradient [Chen et al., 2016; Shay et al., 2016]. Malakit et al. [2013] reported a Larmor electric field E_N pointing toward the magnetosphere on the inflow side of the magnetosheath-pointing E_N during asymmetric reconnection. How the E_N structure in asymmetric reconnection affects the ion motion remains to be addressed.

The meandering motion and the effects of the reconnection (E_M) and polarization (E_N) electric fields are reflected in velocity distribution functions (VDFs). Due to the finite Larmor radius effect during the meandering motion, the out-of-plane fluid velocities of ions (electrons) are biased toward (opposite to) the current direction. The resulting distribution has a crescent shape in the v_M - v_N plane near the magnetic field reversal of a current sheet (not necessarily with reconnection), as shown in observations and simplified models [e.g., Kistler et al., 2005; Wang et al., 2014]. Electron crescent distributions were reported in asymmetric

reconnection simulations [Hesse *et al.*, 2014; Bessho *et al.*, 2016; Chen *et al.*, 2016; Shay *et al.*, 2016], theoretical models [Bessho *et al.*, 2016], and observations [Burch *et al.*, 2016] as a feature of the electron diffusion region with weak guide field. In reconnection, the acceleration by E_M during multiple bounces of particles across the current sheet leads to multiple striations in v_M for symmetric [e.g., Ng *et al.*, 2011; Zenitani *et al.*, 2013; Bessho *et al.*, 2014] and asymmetric reconnection [e.g., Chen *et al.*, 2016]. In addition, Bessho *et al.* [2016] showed that the acceleration by E_N for electrons away from the midplane modifies the shape and the size of a crescent distribution. Close to the midplane, ions bouncing across the current sheet exhibit counter-streaming beams in N [Arzner and Scholer, 2001; Aunai *et al.*, 2011]. Recent magnetotail observations showed the coexistence of low-energy ion counter-streaming beams in v_N and energetic populations with large $|v_M|$, indicating the ion meandering motion [Nagai *et al.*, 2015].

In this study, analysis of ion VDFs in a 2-D particle-in-cell (PIC) simulation of asymmetric reconnection with zero guide field is carried out to show how the cyclotron turning around B_L and the trapping by E_N affect the ion meandering motion and the structure of the ion diffusion region (IDR) close to the X line. VDF features observed near the diffusion region by the magnetospheric multiscale (MMS) mission [Burch *et al.*, 2015], will be shown to be consistent with PIC predictions.

2. Data

The presented simulation has the same setup as in Chen *et al.* [2016] except that the number of particles per cell is doubled to be 6000. Between magnetosheath and magnetospheric sides, the density ratio is 8, the magnetic field strength ratio is 1/1.37, and the temperature ratio is 1. The ion-to-electron temperature ratio (T_i/T_e) is 2. Data in the following analysis are taken at $t\omega_{ci} = 72, 16 \omega_{ci}^{-1}$ after the peak reconnection rate, where ω_{ci} is the ion cyclotron frequency based on the magnetosheath magnetic field B_0 , lengths in unit of the magnetosheath ion skin depth d_i , velocities in the magnetosheath ion Alfvén speed (v_A), and electric fields in $2v_A B_0$.

For MMS observations, ion measurements are from the burst mode Fast Plasma Instrument (FPI) with a 0.15 s time resolution [Pollock *et al.*, 2016]. Magnetic field data are of 128 Hz burst rate from FluxGate Magnetometer, and electric field data are of 32 Hz fast mode from axial and spin-plane double-probe electric field sensors (ADP and SDP) [Torbert *et al.*, 2014].

3. Simulation Results

Figures 1a–1c show the nonideal electric field $E'_M = (E + V_i \times B)_M$, where V_i is the ion bulk velocity, E_N , and the ion degree of nongyrotropy (Dng_i) defined as $2\sqrt{\sum_{ij} N_{ij}^2} / \text{Tr}(\mathbf{P}_s)$, where N_{ij} are nongyrotropic parts of the pressure tensor (\mathbf{P}_s) [Aunai *et al.*, 2013]. Separatrices are marked in grey, intersecting at the X line at $[L, N] = [38.50, -0.15]$. Dng_i is enhanced close to the X line, which appears to be associated with the E_N profile, and their correlation is more clearly shown in the 1-D cuts along N across the X line (Figure 1d). Dng_i has two peaks on the magnetospheric side: an inner peak near the E_N reversal ($N = -0.6$, location D) between the magnetosheath- and the magnetospheric-pointing E_N ; an outer peak (location F) at $N \sim -2.5$. Near both Dng_i peaks, E'_M are negative and show variations along L and N , indicating that L and N components of $\nabla \times E'$ are nonzero, since M is the direction of invariance in the 2-D simulation. The finite $\nabla \times E'$ suggests that the regions near the Dng_i peaks belong to the IDR, where ions are not frozen-in. As will be discussed below, meandering ions exist in VDFs at the Dng_i enhancements, which further confirm the enhanced Dng_i regions to be within the IDR.

Ion behaviors in the IDR are analyzed with VDFs to reveal the effect of E_N . Reduced VDFs (Figure 1e) are shown in the v_M - v_N plane, roughly perpendicular to B . The VDFs are taken at the representative locations in the Dng_i and E_N profiles, marked by white boxes in Figures 1a–1c and dots on curves in Figure 1d, and labeled as A–F in Figure 1a. Each VDF is generated over a spatial size of $0.4d_i \times 0.1d_i$. VDF B in v_L - v_M is shown in Figure 1g, and those at other locations in v_L - v_M and v_L - v_N planes are shown in Figure S1 in the supporting information.

Two main populations stand out above and below the X line in v_M - v_N distributions: a crescent-shaped energetic population with its tip pointing toward the negative v_M direction and a core inflow population.

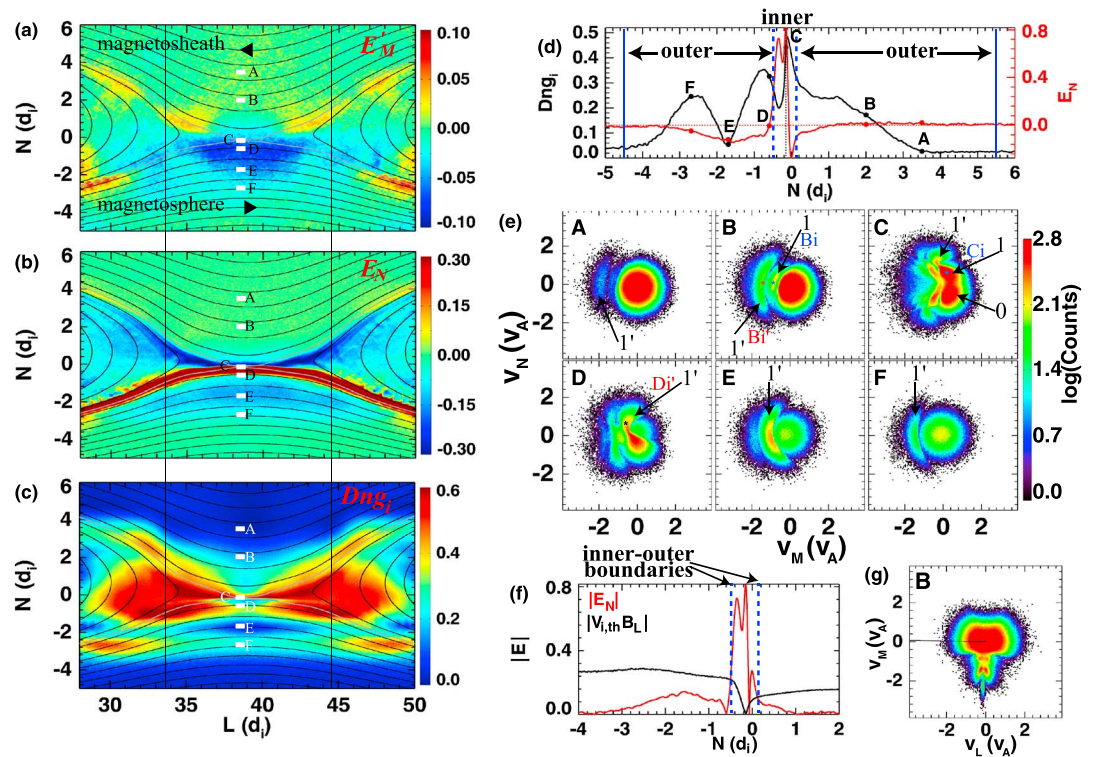


Figure 1. (a) Nonideal electric field $E_M = (E + V_j \times B)_M$, (b) normal electric field (E_N), and (c) ion degree of nongyrotropy (Dng_i). White boxes in each panel mark the locations of VDFs shown in Figure 1e and are labeled as A–F. Vertical lines in Figures 1a–1c mark the boundaries where the two-scale meandering analysis is valid. (d) Dng_i (black) and E_N (red) profiles along N across the X line (black vertical line). (e) Ion VDFs in v_M - v_N at locations marked by dots on curves in Figure 1d. Numbers 0 and 1 label the number of bounces for magnetosheath ions across the current sheet, with 1 and 1' representing the meandering in the inner and outer scales on the magnetospheric side, respectively. Bi, Bi', Ci, and Di' label populations from which test particles shown in Figure 2 are taken. (f) Red: $|E_N|$, black: $|V_{i,th} B_L|$, where $V_{i,th}$ is the local thermal speed $\sqrt{k_B T_i / m_i}$. The crossovers of the two curves mark the inner-outer meandering scale boundaries, marked as blue dashed lines in Figures 1d and 1f. The blue solid vertical lines in Figure 1d mark the boundaries of the outer meandering scale. (g) VDF B in the v_L - v_M plane.

At the X line (C), the inflow population from the magnetosheath (marked as 0) is centered at a positive v_M and a negative v_N , consistent with the $E \times B$ drift velocity direction on the magnetosheath side of the X line around $N = [-0.05, 1]$, with a negative E_N and a negative E_M .

Population 1 in the X line VDF C reflects the effect of the positive E_N . The high counts of population 1 indicate that a significant portion of these ions originally come from the magnetosheath. The ions that have bounced once across the current sheet and are going back to the magnetosheath are labeled as population 1. Blue traces (Ci) in Figures 2a and 2b show the test particle trajectories in the L - N position space and the v_M - v_N velocity space of an ion from this population. The star marked in VDF C (Figure 1e) shows the initial velocity of the traced ions (same for other test particles in VDFs B and D discussed below). Solid curves in test particle results represent the backward tracing, and dashed curves are for forward tracing, both for $6 \omega_{ci}^{-1}$ using time-varying PIC electromagnetic field data interpolated to each tracing step. The ion comes from the magnetosheath and bounces across the current sheet center (Figure 2a). In v_M - v_N (Figure 2b), the sudden change of the velocity at the lower right vertex corresponds to the E_N reversal around $N = -0.05$ (Figure 1d). The last part of the solid trace in Figure 2b, almost a straight line from negative to positive v_N , corresponds to the motion of this ion on the magnetospheric side of the X line (below the horizontal dashed line in Figure 2a). The sharp v_N reversal is due to the large-amplitude positive E_N providing an electric force dominating over the magnetic force, which is representative for the transition from populations 0 to 1 in VDF C. Since E_N is an electrostatic field, $|v_M|$ is conserved before and after the reflection. Thus, population 1 is almost the mirror image of population 0 relative to $v_N = 0$, with only slight changes in v_M .

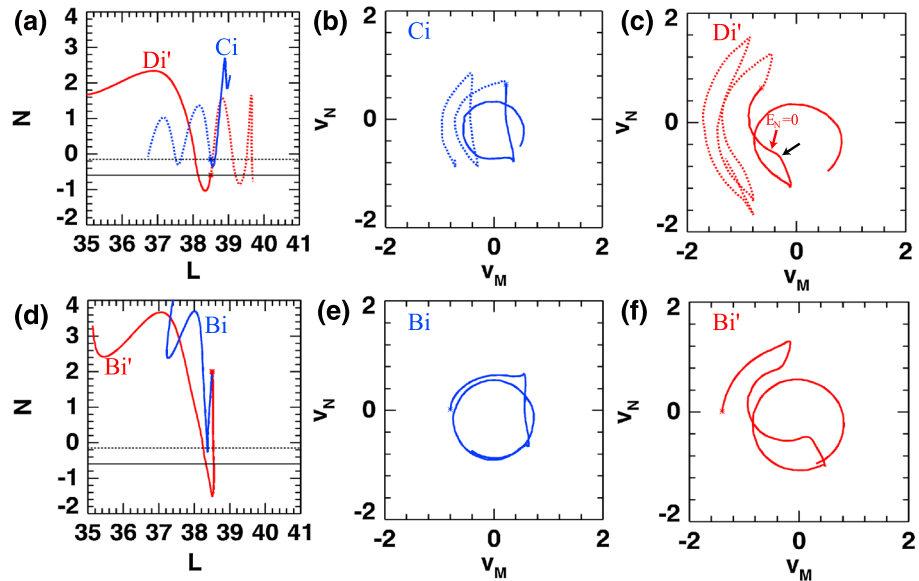


Figure 2. Ion test particle trajectories in the (a and d) L - N position space, and in the (b, c, e and f) v_M - v_N velocity space. Solid lines represent backward tracing result, and dashed lines represent forward tracing results. Initial positions and velocities of particles are marked with stars in each panel as well as in VDFs in Figure 1e. In Figures 2a and 2d, the dashed horizontal line marks the N location of the X line, and the solid horizontal line marks the N location of the E_N reversal marked as D in Figure 1d.

VDF D at the E_N reversal ($N = -0.6$) contains critical information about the E_N effect on the IDR structure. Ions with $v_N > 0$ in population 1' marked in VDF D are coming back to location D from the magnetospheric side after a bounce in the negative E_N region. Red curves (Di') in Figures 2a and 2c show the test particle results of an ion in this population. In v_M - v_N (Figure 2c), a sudden change in the trajectory (marked by the black arrow) occurs as the ion moves toward the magnetosphere with $v_N < 0$ and encounters the sharp gradient of E_N at $N \sim -0.5$, leading to an abrupt acceleration change. Thereafter, the magnetic force becomes dominant over the electric force, and the trajectory in v_M - v_N becomes more circular with slower $|v_N|$ decreases. After encountering the E_N reversal (red arrow in Figure 2c, close to the sudden acceleration change), the negative E_N helps further pull the ions toward the magnetosphere before the ion is cyclotron turned back by the magnetic field and bounces to the observed location.

The critical difference between the above two particles is that during the first bounce from magnetosheath to magnetosphere, Di' can reach the magnetospheric side of the sharp E_N gradient close to its reversal at $N = -0.6$ (horizontal black solid line in Figure 2a). Consequently, Di' bounces in a larger N range, and its v_N reaches a larger amplitude. Trajectories of Ci and Di' are representative of 1000 ions traced in each of the two populations.

The above result indicates a two-scale structure of the ion meandering motion separated by the E_N gradient. To further demonstrate this, Figures 2d-2f show backward tracing (by $9 \omega_{ci}^{-1}$) results of two ions (Bi and Bi') from the two crescents (1 and 1') in VDF B (Figure 1e). Compared to Bi , Bi' bounces at a larger scale in N passing to the magnetospheric side of the E_N gradient. Note that the initial gyrospeeds (radii of circular gyrotrajectories in v_M - v_N) of two particles differ by less than $0.1 v_A$, while after one bounce back to the magnetosheath, $|v_M|$ of ion Bi' is larger than that of Bi by about $0.6 v_A$. The sharp change of the acceleration from inside to outside of the strong positive E_N layer increases the bouncing time for Bi' to be further accelerated by E_M . As such, the negligible difference between the initial velocities of the two populations represented by Bi and Bi' is amplified, so that they appear as discrete crescents in VDF B.

For each ion, the transition between the inner and outer scales of meandering, defined by the dominant trapping force, occurs when $|E_N|$ decreases to $|(v_i \times B)_N|$, where v_i is the ion particle velocity. Statistically, the cross-over between $|E_N|$ and $|V_{i,th} B_L|$ (red and black in Figure 1f), where $V_{i,th} = \sqrt{k_B T_i / m_i}$ is the local thermal speed, represents the boundary between the inner and outer meandering scales (blue dashed lines in Figures 1d

and 1f). Ions bouncing at a larger scale are more efficiently accelerated by the reconnection electric field during one bounce. The populations bouncing at two scales can be distinguished in VDFs (marked by 1 and 1' in Figure 1e, respectively).

The two scales of meandering have corresponding features in VDFs and Dng_i . Near the midplane, since E_N dominates in trapping and accelerates ions toward the midplane, the VDF (e.g., C in Figure 1e) has counter-streaming populations in v_N and is elongated more in N than in M . Note that the nonzero negative v_N of magnetosheath ions comes from both the E_N acceleration and the inflow velocity due to E_M , and the effect of the strong electric force on the magnetospheric side of the X line is to make ions quickly reverse v_N without much change in v_M . In the outer scale, e.g., location F, v_N of meandering ions is cyclotron turned to the M direction, and the resulting VDF becomes crescent shaped, i.e., the distribution of meandering ions is more circular in the outer scale than in the inner scale. The superposition of magnetospheric inflow ions and crescent meandering ions causes the VDF to be elongated more in M than in N . The difference between the thermal spread in M and in N leads to Dng_i enhancements. The inner Dng_i peak roughly marks the boundary between the inner and outer meandering scales (Figure 1d). The outer Dng_i peak is at location F in the outer scale. As the cyclotron turning proceeds in the outer meandering scale, Dng_i exhibits a dip between the two peaks when the thermal spreads in M and N become comparable (e.g., location E).

The VDF features help understand the ion force balance in N . As discussed in a recent simulation study [Shay *et al.*, 2016], where two crescent-like distribution examples in the $E_N < 0$ region were reported (Figures 4f and 4g in their paper), the negative bulk V_M resulting from the crescent along with $B_L > 0$ provides a negative convective part of E_N . In addition, as ions increase $|v_N|$ toward the midplane, the thermal spread of the crescent along N and the velocity separation of counter-streaming populations increase. Together with the increasing density toward the magnetosheath, the variation along N of the NN -component ion pressure is positive on the magnetospheric side of the midplane, supporting the nonideal part of E_N , i.e., $(E + V_i \times B)_N$.

The Dng_i enhancements between $N \sim -4.0$ and $N \sim 3.5$ roughly indicate the meandering scale, while the exact outer boundaries for meandering ions to reach are farther out. For the presented simulation data, the existence of meandering ions in crescent distributions extends to about $N = -4.5$ on the magnetospheric side and $N = 5.5$ on the magnetosheath side, which could be marked as the boundaries of the IDR in N (blue solid vertical lines in Figure 1d). The two-scale meandering motion is valid for about $5 d_i$ from the X line in the L direction (marked by vertical lines in Figures 1a–1c). Further downstream, E_N is strong only near the separatrices and has smaller effects on trapping ions close to the midplane.

During asymmetric reconnection, the asymmetry of positive and negative midplane pointing E_N leads to an asymmetric in-plane electrostatic potential (Figures 1d and 1f). As a result, ions trapped in the inner scale on the magnetospheric side of the midplane may escape to the outer scale on the magnetosheath side where the magnetic force becomes important and the VDF becomes crescent shaped. Population 1 in VDF B is an example: location B is in the outer scale on the magnetosheath side well beyond the E_N gradient; when population 1 moves to the magnetospheric side of the X line, it cannot go beyond the inner-outer scale boundary. Therefore, the double crescent populations corresponding to ions bouncing in the magnetospheric side inner and outer scales during one bounce are a specific feature for the magnetosheath side in asymmetric reconnection.

Such a double crescent distribution corresponds to multiple peaks in v_M (can also be seen in the v_L - v_M plane in Figure 1g). Previous studies [e.g., Ng *et al.*, 2011; Bessho *et al.*, 2014] showed that the E_M acceleration during multiple bounces can lead to multiple peaks in v_M of electron VDFs in the diffusion region. In the examined simulation, ions also get continuous E_M acceleration during multiple bounces, as can be seen from the v_M elongation in Figures 1g and S1a. At location B, the bouncing in different scales dominates over bouncing multiple times in forming two crescents. In contrast, at location E outside of the inner-outer bouncing boundary, the double crescents in VDF E are merely caused by ions bouncing multiple times. At the midplane, counter-streaming ions with different numbers of bounces form multiple stripes at different v_M in VDF C.

The effect of E_M further modifies the VDF structure. In VDF E on the magnetospheric side for example, as ions leave the observation point further to the magnetosphere and bounce back, they get additional acceleration by E_M . Thus, the population with $v_N > 0$ moving toward the midplane is shifted to larger $|v_M|$, and the whole crescent distribution appears as rotated counterclockwise. Due to the same mechanism, the distribution is

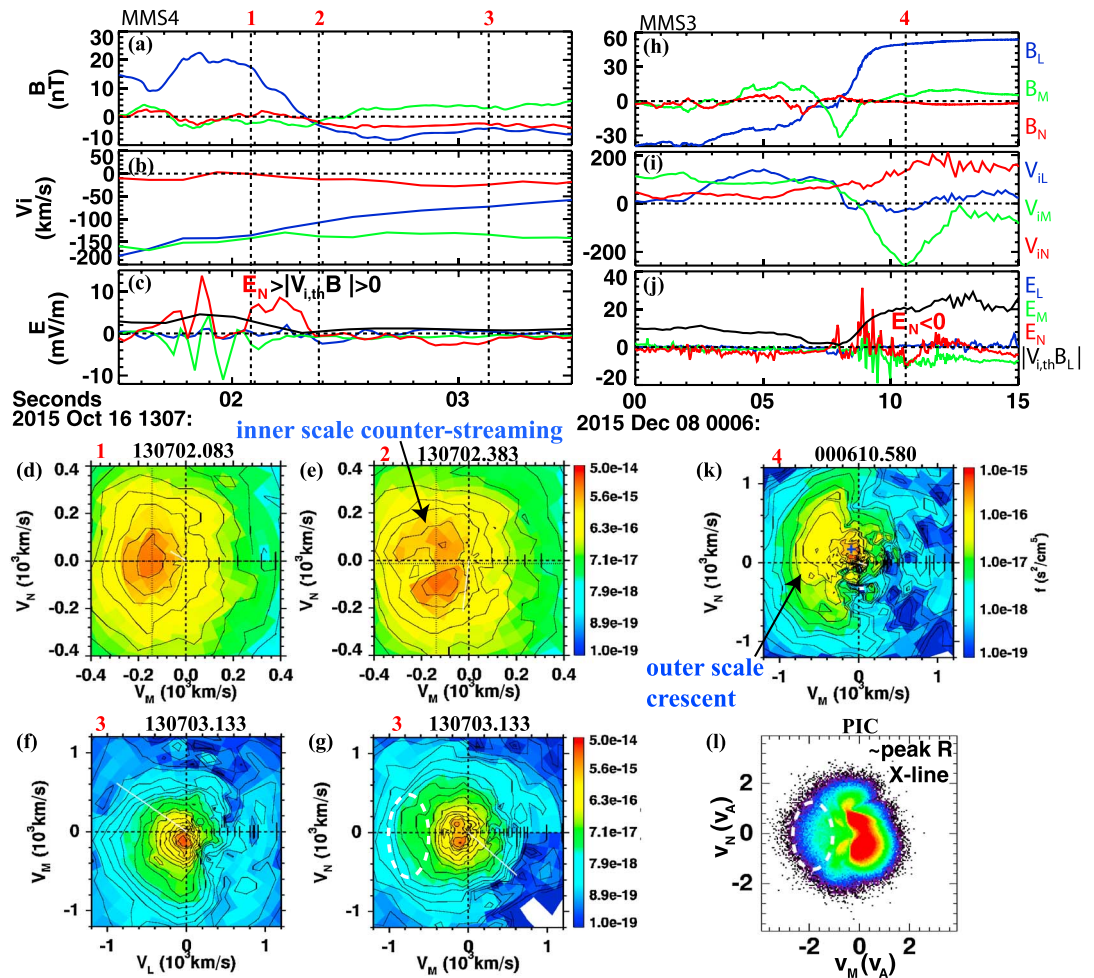


Figure 3. Ion VDFs showing two-scale meandering motion observed by MMS. (a–j) From two magnetopause reconnection events. Figures 3a–3c and 3h–3j show magnetic fields, ion velocities, and electric fields. Black curves in Figures 3c and 3j are $|V_{i,th}B_L|$, where $V_{i,th}$ is the ion local thermal velocity. The comparison $|E_N|$ and $|V_{i,th}B_L|$ indicates the dominance between the electric and magnetic forces. Dashed vertical lines mark the starting time of VDFs shown below. Figures 3d–3g and 3k are reduced VDFs for ions below 18 keV. In each VDF panel, the dashed line marks the zero velocity, and the white line marks the in-plane magnetic field direction. Dotted lines in Figures 3d and 3e mark the in-plane bulk velocity. (l) PIC ion VDF at the X line close to the time of the peak reconnection rate (R), where the white oval highlights the population with large- $|v_M|$ and small- $|v_N|$ that does not exist in VDF C of Figure 1e, and observed in the MMS VDF (Figure 3g).

rotated in the opposite direction at locations A and B on the magnetosheath side. Therefore, the rotation of the crescent distribution serves as evidence for the acceleration by E_M .

The two-scale meandering depends on the temporal evolution of reconnection and only exists after the E_N structure is well developed. For the examined asymmetric simulation, the sharp E_N gradient is developed around $8 \omega_{ci}^{-1}$ before the peak reconnection rate, before which the amplitude of the positive E_N on the magnetospheric side does not exceed local $|V_{i,th}B_L|$ anywhere (not shown). As a result, the magnetic force dominates throughout the meandering motion.

The VDF feature reflects the electric field evolution. In VDF C, all stripes exhibit counter-streaming signatures with few counts near zero v_N at $|v_M|$ greater than $\sim 1.2 V_A$. The VDF in Figure 3l is at the X line close to $(4 \omega_{ci}^{-1})$ after the peak reconnection rate. The counter-streaming feature is only clear for populations with small $|v_M|$, while there are many energetic ions whose $|v_N|$ is close to zero (marked by a white dashed oval). In the VDF, $|v_M|$ reflects acceleration time due to E_M . The ions with larger $|v_M|$ indicate that they entered this region in earlier time and have been accelerated by E_M for a long time. In Figure 3l, $|v_M|$ of the large- $|v_M|$ population is small, because the reconnection inflow speed, which affects $|v_M|$ of those ions, was small when the reconnection rate at the early

time was small. Therefore, in this VDF, we do not see the stripes at larger $|v_M|$ as in VDF C, (the large $|v_N|$ is due to the large reconnection inflow in well-developed reconnection). In the later time (VDF C), there are no populations with large $|v_M|$ and small $|v_N|$, because they have been already ejected out to the downstream. Therefore, the lack of ions with large $|v_M|$ and small $|v_N|$ at the midplane suggests that the reconnection is well developed.

4. Observation Results

Counter-streaming and crescent ion VDFs and E_N structures are observed by MMS. Figures 3a–3g show an electron diffusion region encounter on 16 October 2015 [Burch *et al.*, 2016]. This event has a density ratio of 16, a reconnecting magnetic field ratio of 1/1.2, a relatively weak guide field of 15% of the magnetosheath reconnecting component of the magnetic field, and T_i/T_e of about 10 in the magnetosheath. Figures 3a–3c show the magnetic field, ion velocity, and electric field, and dashed vertical lines mark the starting time of each frame for ion VDFs in Figures 3d–3g.

VDFs 1–2 (Figures 3d and 3e) are from the times when electrons present crescent distributions, indicating close proximity to the electron diffusion region [Burch *et al.*, 2016]. Close to the B_L reversal (VDF 2), ions exhibit well-separated counter-streaming v_N centered around ± 80 km/s, while v_M for the two populations are similar around the bulk velocity of -150 km/s (vertical dotted line), which is the bulk V_M in the magnetosheath proper [Burch *et al.*, 2016]. The phase space density difference between counter-streaming populations and those with near-zero v_N is confirmed to be greater than the statistical error (not shown). Moving toward the magnetosphere with increasing B_L , counter-streaming populations exhibit much smaller $|v_N|$ and can no longer be clearly distinguished as two populations at VDF 1. Importantly, v_M of these ions does not change much from that in VDF 2, i.e., the effect of the velocity conversion from v_N to v_M during the gyration around B_L is small. Such a transition is similar with that from simulation VDFs C to D in Figure 1e, as a result of the trapping dominant by E_N . The positive E_N enhancement is, in fact, observed during these two time frames (red in Figure 3c). E_N is greater than $|V_{i,th} B_L|$ (black in Figure 3c), suggesting a dominant electric force over the magnetic force.

VDF 3 (Figure 3f and 3g) corresponds to the time when V_{iL} is equal to that in the magnetosheath proper, -78 km/s. The average B_L during this frame is -4.6 nT, only about 16% of the magnetosheath B_L . Thus, location 3 is close to the X line in the L direction and is also close to the midplane. Counter-streaming ions can be seen in the v_M - v_N plane (Figure 3g). The distribution also exhibits elongation toward $-v_M$ up to about -900 km/s around the same v_L with low-energy ions (3f) and has nearly zero v_N (3g). The v_M elongation serves as the evidence of acceleration by E_M . Such a high- $|v_M|$ and low- $|v_N|$ population (highlighted by the white dashed oval) exists throughout the shown interval after location 2 where B_L is close to zero. Its coexistence with counter-streaming v_N ions (3g) is similar with the PIC VDF in Figure 3l, suggesting that high- $|v_M|$ ions entered the current sheet in the early reconnection phase and have not been ejected yet. According to the simulation result, the reconnection in this MMS event may not be much later than the peak reconnection rate.

Figures 3h–3l show another magnetopause crossing on 8 December 2015. In this event, the density ratio is around 22, the reconnecting magnetic field ratio is 1/1.35, the guide field is 13% of the magnetosheath reconnecting magnetic field, and T_i/T_e in the magnetosheath is 8. The background magnetosheath V_{iL} is close to zero (Figure 3i, $\sim 00:06:00$ UT). VDF 4 (Figure 3k) is taken from the magnetospheric side with a negative V_{iM} peak and negative E_N (Figures 3i and 3j). A population with small positive v_N and negative v_M are magnetospheric cold ions following the $E \times B$ drift velocity (marked by the blue cross at $v_M = -92$ km/s and $v_N = 165$ km/s). A hotter population from the magnetosheath (yellow in color) forms a crescent distribution at negative v_M . At location 4, the bulk V_{iL} is close to zero (Figure 3i), and both magnetospheric cold ions and magnetosheath ions are centered around zero v_L in the VDF (not shown), suggesting the location not far from the X line. Therefore, the crescent magnetosheath ion distribution together with $E_N < 0$ provide evidence for the outer meandering scale predicted by PIC.

5. Conclusions

In this study, we present ion VDFs along N across the X line in an asymmetric reconnection simulation. The ion meandering orbit close to the X line is found to have two scales, separated by the inflow side gradient of the

midplane pointing E_N . Ions bouncing in the inner region are mainly trapped by E_N , while those reach the outer scale are turned back mainly by the magnetic force. In the inner scale close to the midplane, the ion VDF exhibits counter-streaming populations with similar distributions to each other. Within the inner scale, $|v_N|$ of the counter-streaming populations decreases away from the midplane due to E_N without changing v_M , and the VDF exhibits elongation along v_N . In the outer scale, v_N of ions is cyclotron turned to v_M by the magnetic force and VDFs present crescent shapes. Dng_i has a peak around the E_N gradient near the inner-outer scale boundary and an additional peak farther out because of the superposition of crescent VDFs of meandering ions and inflow populations. During asymmetric reconnection, due to the asymmetry in the midplane pointing E_N on the magnetospheric and magnetosheath sides, ions can be trapped in the inner scale on the magnetospheric side while bounce to the outer scale on the magnetosheath side.

Observations of counter-streaming ions near the B_L reversal with decreasing $|v_N|$ away from the midplane and little change in $|v_M|$, together with an observed strong positive E_N on the magnetospheric side, provide evidence for the meandering of ions dominantly trapped by E_N . Ions with high- $|v_M|$ and low- $|v_N|$ are results of acceleration by E_M . In a different event, crescent distributions of magnetosheath ions are observed on the magnetospheric side with negative E_N , consistent with the outer-scale meandering. The results suggest that the ion two-scale meandering structure predicted in the PIC simulation is applicable to magnetopause observations.

Acknowledgments

The research is supported in part by NSF grants AGS-1543598, AGS-1202537, and AGS-1552142 and NASA grants to the MMS Theory and Modeling and FPI at GSFC. IRAP contribution to MMS was supported by CNES and CNRS. MMS data are available at MMS Science Data Center (<https://lasp.colorado.edu/mms/sdc/>).

References

- Arzner, K., and M. Scholer (2001), Kinetic structure of the post plasmoid plasma sheet during magnetotail reconnection, *J. Geophys. Res.*, *106*, 3827–3844, doi:10.1029/2000JA000179.
- Aunai, N., G. Belmont, and R. Smets (2011), Proton acceleration in antiparallel collisionless magnetic reconnection: Kinetic mechanisms behind the fluid dynamics, *J. Geophys. Res.*, *116*, A09232, doi:10.1029/2011JA016688.
- Aunai, N., M. Hesse, and M. Kuznetsova (2013), Electron nongyrotropy in the context of collisionless magnetic reconnection, *Phys. Plasmas*, *20*(9), 092903, doi:10.1063/1.4820953.
- Bessho, N., L.-J. Chen, J. R. Shuster, and S. Wang (2014), Electron distribution functions in the electron diffusion region of magnetic reconnection: Physics behind the fine structures, *Geophys. Res. Lett.*, *41*, 8688–8695, doi:10.1002/2014GL02034.
- Bessho, N., L.-J. Chen, and M. Hesse (2016), Electron distribution functions in the diffusion region of asymmetric magnetic reconnection, *Geophys. Res. Lett.*, *43*, 1828–1836, doi:10.1002/2016GL067886.
- Burch, J. L., T. E. Moore, R. B. Torbert, and B. L. Giles (2015), MMS overview and science objectives, *Space Sci. Rev.*, doi:10.1007/s11214-015-0164-9.
- Burch, J. L., et al. (2016), Electron-scale measurements of magnetic reconnection in space, *Science*, doi:10.1126/science.aaf2939.
- Chen, L.-J., W. S. Daughton, B. Lefebvre, and R. B. Torbert (2011), The inversion layer of electric fields and electron phase-space-hole structure during two-dimensional collisionless magnetic reconnection, *Phys. Plasmas*, *18*(1), 012904, doi:10.1063/1.3529365.
- Chen, L.-J., W. S. Daughton, A. Bhattacharjee, R. B. Torbert, V. Roytershteyn, and N. Bessho (2012), In-plane electric fields in magnetic islands during collisionless magnetic reconnection, *Phys. Plasmas*, *19*, 112902, doi:10.1063/1.4767645.
- Chen, L.-J., M. Hesse, S. Wang, N. Bessho, and W. S. Daughton (2016), Electron energization and structure of the diffusion region during asymmetric reconnection, *Geophys. Res. Lett.*, *43*, 2405–2412, doi:10.1002/2016GL068243.
- Fujimoto, K. (2006), Time evolution of the electron diffusion region and the reconnection rate in fully kinetic and large system, *Phys. Plasmas*, *13*, 072904, doi:10.1063/1.2220534.
- Hesse, M., N. Aunai, D. Sibeck, and J. Birn (2014), On the electron diffusion region in planar, asymmetric, systems, *Geophys. Res. Lett.*, *41*, 8673–8680, doi:10.1002/2014GL061586.
- Kistler, L. M., et al. (2005), Contribution of nonadiabatic ions to the cross-tail current in an O^+ dominated thin current sheet, *J. Geophys. Res.*, *110*, A06213, doi:10.1029/2004JA010653.
- Lavraud, B., et al. (2016), Currents and associated electron scattering and bouncing near the diffusion region at Earth's magnetopause, *Geophys. Res. Lett.*, *43*, 3042–3050, doi:10.1002/2016GL068359.
- Liu, Y. H., C. G. Mouikis, L. M. Kistler, S. Wang, V. Roytershteyn, and H. Karimabadi (2015), The heavy ion diffusion region in magnetic reconnection in the Earth's magnetotail, *J. Geophys. Res. Space Physics*, *120*, 3535–3551, doi:10.1002/2015JA020982.
- Malakit, K., M. A. Shay, P. A. Cassak, and D. Ruffolo (2013), New electric field in asymmetric magnetic reconnection, *Phys. Rev. Lett.*, *111*, 135001, doi:10.1103/PhysRevLett.111.135001.
- Nagai, T., I. Shinohara, and S. Zenitani (2015), Ion acceleration processes in magnetic reconnection: Geotail observations in the magnetotail, *J. Geophys. Res. Space Physics*, *120*, 1766–1783, doi:10.1002/2014JA020737.
- Ng, J., J. Egedal, A. Le, W. S. Daughton, and L.-J. Chen (2011), Kinetic structure of the electron diffusion region in antiparallel magnetic reconnection, *Phys. Rev. Lett.*, *106*(6), 065002, doi:10.1103/PhysRevLett.106.065002.
- Pollock, C., et al. (2016), Fast plasma investigation for magnetospheric multiscale, *Space Sci. Rev.*, doi:10.1007/s11214-016-0245-4.
- Shay, M. A., T. D. Phan, C. C. Haggerty, M. Fujimoto, J. F. Drake, K. Malakit, P. A. Cassak, and M. Swisdak (2016), Kinetic signatures of the region surrounding the X-line in asymmetric (magnetopause) reconnection, *Geophys. Res. Lett.*, *43*, 4145–4154, doi:10.1002/2016GL069034.
- Shuster, J. R., L.-J. Chen, M. Hesse, M. R. Argall, W. S. Daughton, R. B. Torbert, and N. Bessho (2015), Spatiotemporal evolution of electron characteristics in the electron diffusion region of magnetic reconnection: Implications for acceleration and heating, *Geophys. Res. Lett.*, *42*, 2586–2593, doi:10.1002/2015GL063601.
- Torbert, R. B., et al. (2014), The FIELDS Instrument Suite on MMS: Scientific objectives, measurements, and data products, *Space Sci. Rev.*, doi:10.1007/s11214-014-0109-8.
- Wang, S., L. M. Kistler, C. G. Mouikis, Y. Liu, and K. J. Genestreti (2014), Hot magnetospheric O^+ and cold ion behavior in magnetopause reconnection: Cluster observations, *J. Geophys. Res. Space Physics*, *119*, 9601–9623, doi:10.1002/2014JA020402.

Wygant, J. R., et al. (2005), Cluster observations of an intense normal component of the electric field at a thin reconnecting current sheet in the tail and its role in the shock-like acceleration of the ion fluid into the separatrix region, *J. Geophys. Res.*, *110*, A09206, doi:10.1029/2004JA010708.

Zenitani, S., I. Shinohara, T. Nagai, and T. Wada (2013), Kinetic aspects of the ion current layer in a reconnection outflow exhaust, *Phys. Plasmas*, *20*, 092120.